Rivista Italiana di Filosofia Analitica Junior Vol 14, No. 2 (2023)
ISSN: 2037-4445

Texture Analysis and Support Vector Machine for Classifying SEM images of VA-CNTs

Hamed Jabbari

Department of Electrical Engineering, Faculty of Technical and Engineering, Imam Khomeini International University, Qazvin, Iran

Corresponding author

***Nooshin Bigdeli**

Department of Electrical Engineering, Faculty of Technical and Engineering, Imam Khomeini International University, Qazvin, Iran

Amire Seyedfaraji

Department of Electrical Engineering, Faculty of Engineering, Alzahra University, Tehran, Iran

Abstract

Dispersion of Carbon Nanotubes (CNTs) is one of the most substantial indicators designed to verify the effectiveness of the proposed methods in synthesizing CNTs. In recent years, various approaches have been suggested to synthesize nanostructures in which Scanning Electron Microscopy (SEM) has been used to demonstrate the quality of the CNTs. The SEM images of CNTs contain critical information with high resolution on a nanometer scale. The dispersion degree detection is one of the challenges in the quality of dispersion's CNTs. If SEM images of CNTs have uniform and agglomerated distributions of particles, they are called sparse and dense images, respectively. Thus, the CNT images can be classified into two categories, including dense and sparse images. In the present study, a new algorithm has been developed to classify vertically aligned CNTs (VA-CNTs) based on texture analysis and Support Vector Machine (SVM). In this regard, these images were first transformed to time series, and their specifications were investigated through time series and Gray-Level Co-Occurrence Matrix (GLCM) analysis methods. Then, statistical specifications of these series were extracted. In this case, eight features have been extracted to classify VA-CNTs. The extracted specifications were used as inputs of an SVM algorithm to classify SEM images of CNTs into two groups, entailing dense and sparse. This algorithm has been tested on 80 VA-CNTs images with identical sizes. The findings showed a precision above 98 percent, which proved the validity of the proposed algorithm.

Keywords: VA-CNTs; Agglomeration; SEM Image; Texture Analysis; Time Series Analysis; SVM Algorithm

1 Introduction

Carbon Nanotubes (CNTs) are one of the most widely used carbon structures [1]. The discovery of CNTs has caused extensive research activities in sciences, and researchers have investigated carbon nanostructures and their applications. The principal reason for this issue arises from the CNTs' expected structural evolution, small size, low dispersion, high hardness, and high strength. Besides, they provide a great specific surface area due to their high aspect ratio [2], which is the key property in sensor manufacturing applications. As a result, carbon nanotubes are widely used in material reinforcement [3], flat-screen display with field propagation [4], chemical sensors [5], drug delivery [6], and Nano-electronics [7].

CNTs are long, hollow cylindrical tubule structures made of graphite sheets with diameters ranging from below 1 nm to 10 s of nm [8]. The carbon nanotubes are classified based on the number of their carbon layers. Thus, there are two types of CNTs, including single- and multi-walled carbon nanotubes. Single-walled carbon nanotubes (SWCNTs) consist of a single graphene layer and a diameter between 0.4

and 2 nm and usually occur as hexagonal-packed bundles. Multi-walled carbon nanotubes (MWCNTs) include two or several cylinders, each made up of graphene sheets. The diameter of MWCNTs varies from 1 to 3 nm [9].

The application of CNTs in advanced materials and devices has broadly been explored, maturing already in the first decade of the 21st century [10]. There are practical examples for CNTs in various fields, such as chemical sensors [11], carbon fiber reinforced polymer composites [12], wafer-scale electronics [13], electron sources [14], light-emitting diodes (LEDs) [15], flexible electronics [16], and solar cells [17]. Also, it is necessary to mention their applications in biomedicine and health, such as removal of contaminants in drinking water, tissue engineering, and biomedical and biosensing applications [10].

There are several methods to produce nanotubes [18-20], such as laser ablation [21, 22], arc discharge [23], and chemical vapor deposition (CVD) [24]. Among these methods, the CVD technique is easy and cost-effective. This technique can produce high-quality, defect-free, and large-scale CNT. Besides, it is possible to control various parameters involved in CVD experiments [25, 26].

In addition, it is possible to extend the nanotubes by placing catalysts on surfaces. The carbon nanotubes growth mechanism is often such that carbon atoms are transferred, absorbed, dissolved, or released in the catalyst particles or around the catalyst particle surface to grow solid graphite particles on the catalyst surface [27, 28]. This anisotropic and 3D macroporous morphology is called vertically aligned CNTs (VA-CNT). It renders high electrical conductivity and mechanical, chemical, and electrochemical stabilities. These situations cause their broad applications in supercapacitors, electronic interconnects, 28 emitters, dry adhesives, mechanical materials, separation membranes, advanced yarns and fabrics, black-body absorption, high-resolution printing stamps, optical rectennas, chemically driven thermopower waveguides, and ultrasensitive virus detection [29].

Scanning Electron Microscopy (SEM) uses electron bombardment and provides images of objects and 10 nanometers for study [30]. The morphology analysis is recognized as one of the most significant applications of the resulting images. This analysis is carried out on the shape, size, and positioning of particles at a nanoscale [31-33]. The SEM images have often been used to show the quality of the resulting CNTs and their characterization [34-36]. One of the challenging issues to analyze the quality of CNTs is associated with determining the dispersion of the produced CNTs from SEM images [37], particularly VA-CNTs [38, 39]. In some images related to VA-CNTs, nanotubes are distributed over the substrate with uniform gaps throughout the substance. This order is not present in some other images. Also, nanotubes may be clinging, compacted, or less dispersed. This situation significantly affects their specific surface area property. Therefore, the SEM images of VA-CNTs coverage over a substrate can be classified into two categories, encompassing dense and sparse images. Henceforward, the same properties in images are known as dense and sparse CNTs. For example, Fig. 1 depicts two SEM images of dense and sparse CNTs. In this figure, Fig. 1(a) and (b) show sparse and dense CNTs, respectively.

Generally, the CNT images are visually classified from the dispersion viewpoint. Although this procedure is performed via an experienced expert, it is not easy in some cases. Besides, the CNTs are classified based on the hybridization state, [H]/[C] atomic ratio [40], or size [41]. However, this classification process is limited to the structural and apparent features, which does not consider inherent quantitative features in CNTs, like other mentioned references. Although researchers have attempted to classify these images, the literature survey demonstrated that the previous studies did not suggest a suitable set of appropriate features and a convenient way to categorize VA-CNT images automatically (i.e., without the need for an experienced expert). The present study proposes a new method to classify VA-CNTs SEM images based on texture analysis and Support Vector Machine (SVM) algorithm. In this regard, the SEM images of VA-CNTs were initially converted into the time series. Then, the statistical features of their time series and the Gray-Level Co-Occurrence Matrix (GLCM) features of VA-CNT images are extracted and analyzed. Since the time series extracted from each SEM image of VA-CNTs

is unique, it is possible to find features that illustrate the properties and structural characteristics of VA-CNTs. In this case, various statistical and GLCM features extracted from the resulting time series and VA-CNT images are examined. Thus, eight proper features were determined to categorize the SEM images of CNTs. These features include standard deviation (STD), Pearson law (PL), skewness (Sk), smoothness (Sm), interquartile range (IQR), energy 1 (E1), energy 3 (E3), and correlation 2 (Corr2).

In the present study, the SVM method has been accomplished to evaluate the dispersion of VA-CNT images. This method implements a high accuracy separation due to the application of preliminary data. Also, it determines whether the VA-CNT images can be separated based on the dispersion or not. In addition, it demonstrates how SVM can accurately separate these images.

In this case, 80 same-size SEM images of VA-CNTs are used to ensure the accuracy of the proposed method. These images are in dimensions of 540×340 pixels and taken by a Field Emission Scanning Electron Microscope (FE-SEM, Hitachi S-4160, Japan). The results showed that the proposed algorithm had a precision above 98% in classifying the mentioned images. Also, the obtained accuracy and observed error analysis in the algorithm output showed the efficiency of the proposed algorithm in classifying the SEM images of nanoparticles.

This paper is organized as follows. Section 2 expresses the methodology of VA-CNTs image classification. In this section, the texture analysis (i.e., the time series and the GLCM analysis of VA-CNTs images) is first discussed to determine appropriate features, and then the SVM algorithm is reviewed. Also, the confusion matrix and receiver operating characteristic (ROC) curve are employed to evaluate the model validity. Section 3 presents the results and related discussions. Also, the error analysis is performed for the proposed algorithm. Finally, conclusions are summarized in Section 4.

2 Methodology

This study proposes a new method for the automated classification of SEM images of VA-CNTs. The step-by-step study procedure is illustrated in the block diagram of Fig. 2. As shown in this Fig. 2, the required phases for classifying VA-CNT images are as follows:

1. Converting VA-CNT images to a time series

2. Texture analysis, including the extraction of statistical features of the time series and GLCM features of VA-CNT images

3. Applying the proper features as inputs of an SVM algorithm to classify the corresponding image

Therefore, the first step is to present texture analysis, including the time series and GLCM analyses. Then, the SVM algorithm is introduced, and finally, the confusion matrix and ROC curve are considered to evaluate the performance of the proposed algorithm.

2.1 Texture Analysis

Texture analysis is recognized as one of the most crucial issues in image processing and machine vision [42]. Overall, textures are the principal constituents of images. Indeed, textures and features are used to detect, interpret, and classify images.

Different methods have been developed to extract features from texture images [43]. Feature extraction is the most vital step in texture analysis and classification. Also, region description schemes play a significant role in various image analyses and understanding. In the present study, textural features are achieved in two ways: (I) the statistical features of the time series and (II) Gray Level Co-occurrence Matrix (GLCM) of VA-CNT images.

2.1.1 The Time Series Analysis

A time series is a set of observations and statistical data collected in regular intervals or sequential order and sequencing [44]. The time series analysis involves analyzing numerical data and extracting their specific features. The SEM images of VA-CNT are supposed to be converted into a time series to

investigate their properties. In this regard, the basic image processing concepts are used to conduct this procedure. This technique can easily be implemented in MATLAB software. Every three-dimensional image (e.g., the SEM image of a nanostructure) is a three-dimensional matrix of numbers so that each of them denotes red, green, and blue colors, respectively. Depending on the color intensity of each pixel, a number from 0 to 255 is assigned to each dimension. In this case, the numbers "0" and "255" are used for the darkest and brightest pixels, respectively. If the stored matrix numbers are arranged in column and row, the ordered data of the pixels are obtained, which indicate the dispersion of the color intensity of images. This pixel arrangement approach provides a sequence of numbers called the time series of SEM images. This time series is formulated as Eq. (1).

$$X = [D_1 \quad D_2 \quad D_3] \tag{1}$$

where

$$D_i = \left[{C_1}^T \quad {C_2}^T \quad \dots \quad {C_j}^T\right] \tag{2}$$

where *i*=1, 2, 3 is the image dimension, and C_j is the j^{th} column from pixels of each dimension. Fig. 3 depicts an example for the time series of VA-CNT images in Fig. 1. Since there is a unique time series in each SEM image of VA-CNT, it is possible to examine the properties from its time series.

There are various tools and features for analyzing and comparing time series. Statistical features are recognized as the most significant tool for the analysis process. Over the years, different statistical features were examined to show the differences in the time series related to SEM images of VA-CNT. These features are mean, mode, median, covariance, moment, standard deviation, smoothness, Pearson law, entropy, IQR, skewness, and kurtosis (Table 1). Since these features are well-known statistical features, their calculation details have been ignored in this paper.

2.1.2 GLCM Analysis

Generally, some of the texture measures are taken from the GLCM. Besides, the GLCM is a robust method developed to calculate the first- and second-order texture features from the images [45]. Also, it is known as the gray-level spatial dependence matrix, and thus it is a statistical method that examines texture considering the spatial relationship of pixels. Every element (*i, j*) in the resulting GLCM is simply the sum of the number of times that the pixel with the value *I* occurred in the specified spatial connection to a pixel with the value *j* in the input image. In the present study, four matrices corresponding to two different directions (i.e., θ = 0, θ = 45°, θ = 90°, and θ = 135°) and one distance (i.e., *d* = 1 pixel) are computed for each selected mammographic image. These textural features are introduced in Table 1.

2.2 SVM Algorithm

Machine learning is one of the most widely used branches of artificial intelligence [46]. Machine learning techniques teach or learn complex information and carry out future predictions through the learned pattern or rules. The classification problem is one of the principal issues in machine learning, and many problems can be solved as a classification problem. Overall, machine learning employs various methods to solve the classification problem. Among these methods, the support vector machine (SVM) method is one of the most widely used techniques for classification problems. Besides, machine learning methods are utilized to classify images. These methods use automated algorithms to emulate the learning capabilities of the human brain. Also, they play a crucial role in disassembling complex data in many scientific disciplines.

The SVM algorithm is one of the supervisory learning methods used for classification and regression. In this method, it is assumed that no knowledge is available for the distribution of datasets. This algorithm identifies and distinguishes complex patterns in the data and classifies them [47]. If the data are linearly separated (i.e., one or more lines can create a gap between the data), a hyperplane with the maximum margin is obtained to separate the classes. In contrast, if the data are not linearly separated, they are mapped to a more dimensional space to be separated linearly in the new space. If

the training set $(x_i, y_i),\ i = 1, 2, \dots, n,\ x_i \in R^d,\ y_i = \pm 1$ is linearly inseparable, the optimal problem of the separating hyperplane $H: w^T x + b = 0$ is obtained by Eq. (3) [47].

$$\begin{aligned} &\min \frac{1}{2}\|w\|^2 + C\sum_{i=1}^{n}\xi_i \\ &subject\ to\ \ y_i(w^T\varphi(x_i) + b) \geqslant 1 - \xi_i \quad , \quad i = 1, 2, \dots, n \\ &\qquad\qquad \xi_i \geqslant 0 \ , \quad i = 1, 2, \dots, n \end{aligned} \tag{3}$$

where $C > 0$ is the penalty parameter of the error term. Also, the dual problem of quadratic programming is attained by Eq. (4).

$$\begin{aligned} &\max \sum_{i=1}^{n}\alpha_i - \frac{1}{2}\sum_{i,j=1}^{n}\alpha_i\alpha_j\, y_i y_j {x_i}^T x_j \\ &subject\ to\ \ \sum_{i,j=1}^{n}\alpha_i\, y_i = 0 \\ &\qquad 0 \leqslant \alpha_i \leqslant C \quad , \quad i = 1, 2, \dots, n \end{aligned} \tag{4}$$

Using a nonlinear mapping: $\phi: X \to Z,\ X \in R^d, Z \in R^k, k \geqslant d$, the maps input samples $x_i \in X$ into k-dimensional feature space Z. In this situation, the kernel function is $k(x_i, x_j) = \varphi^T(x_i)\varphi(x_j)$. Also, the optimal function is formulated by Eq. (5).

$$\mathrm{Q}(\alpha) = \sum_{i=1}^{n}\alpha_i - \frac{1}{2}\sum_{i,j=1}^{n}\alpha_i\alpha_j\, y_i y_j\, \varphi^T(x_i)\varphi(x_j) = \sum_{i=1}^{n}\alpha_i - \frac{1}{2}\sum_{i,j=1}^{n}\alpha_i\alpha_j\, y_i y_j\, K(x_i, x_j) \tag{5}$$

Finally, the final decision function is as follows:

$$f(x) = \mathrm{sgn}(\sum_{i=1}^{n}\alpha_i^*\, y_i\, K(x_i, x) + b^* \tag{6}$$

One of the principal features of SVM is the data classification based on the minimization of structural errors or the test error [48]. Other classification approaches are often based on minimizing experimental or education errors. In this study, the SVM method was implemented to evaluate the dispersion of VA-CNT images.

2.3 Evaluating the Model Validity

The proposed method has been evaluated using several criteria such as confusion matrix and ROC curve. This procedure has been performed to ensure the correctness of the SVM algorithm. Since the classification is based on the number of images in the correct class, correctness is obtained. In this case, the higher number causes more correctness and proper classification. In other words, images that fall into false categories are characterized as classification errors, and the degree of classification error is a criterion for evaluating the model validity.

Evaluation of classification results is one of the critical steps after implementing each classification process. This procedure is commonly carried out through a set of test samples and the formation of an error matrix. Table 2 introduces the error matrix [49]. This matrix displays how the classification algorithm behaves according to the input dataset and separates the classification problem categories. The False Negative (FN) is the number of records so that their real class is positive, and the classification algorithm wrongly detects their class. The True Negative (TN) is the number of records so that their real class is negative, and the classification algorithm correctly detects their class. The True Positive (TP) is the number of records so that their real class is positive, and the classification algorithm

correctly detects their class. The False Positive (FP) is the number of records so that their actual class is negative, and the classification algorithm wrongly detects their class.

The most crucial criterion to determine the efficiency of a ranking algorithm is the accuracy or classification accuracy rate. This criterion calculates the total accuracy of a classifier. Indeed, it is the most popular criterion for calculating the efficiency of classification algorithms. In other words, it shows that the designed classifier correctly classifies what percent of the total set of test records. Table 2 gives various information, including the sensitivity or True Positive Rate (TPR), fall-out or False Positive Rate (FPR), specificity, and accuracy. These terms are mathematically formulated as follows:

$$TPR = \frac{TP}{TP + FN} \tag{7}$$

$$FPR = \frac{FP}{FP + TN} \tag{8}$$

$$Specificity = \frac{TN}{FP + TN} \tag{9}$$

$$Accuracy = \frac{TP + TN}{TP + TN + FP + FN} \tag{10}$$

In this regard, accuracy indicates the total number of correct prediction ratios. Besides, sensitivity is the ratio of positive cases that are correctly identified. Also, specificity is the ratio of negative cases that are correctly classified. In addition, the FPR is the ratio of negative cases that have been classified incorrectly.

The ROC curve is one of the proper methods to evaluate the results obtained from a classifier and assess its ability to identify the intended class. This procedure is performed to examine the sensitivity of the proposed method [50]. The mean of sensitivity is the relationship between the classified correct and wrong cells. The greater deviation from the baseline for greater ROC identification leads to a more efficient classification process. In addition to investigating the trend of the desired class curve, the area under the curve is calculated. This range represents the probability that a chosen cell is randomly classified correctly. In this case, a longer range shows the method's reliability. Indeed, this curve demonstrates the TPR variability against the FPR. Moreover, MATLAB software has been used to plot this curve.

3 Results and Discussion

As mentioned before, a new method has been developed to classify images using texture analysis and support vector machine algorithms. This classification is based on the amount of accumulation and the dispersion of carbon nanotubes in the images. Therefore, these images are divided into two categories: dense and sparse. However, all of the mentioned features were calculated for 80 SEM images of VA-CNT, including 40 dense and 40 sparse images. These general results are provided in Table 3. For GLCM features, indexes 1, 2, 3, and 4 are related to angles zero, 45, 90, and 135, respectively. According to these results, the eight mentioned features showed a separation process better than the calculated features. The results of these features are discussed in the following paragraphs.

Fig. 4 and Table 4 and Fig. 5 and Table 5 express a few sparse and dense VA-CNTs SEM images with their features, respectively. According to these results, it is observed that the VA-CNTs in the images distributed uniformly are more dispersed than in the images attached and agglomerated to the nanoparticles. Indeed, dense images have a standard deviation lower than sparse images. Also, the skewness absolute value in sparse images is more than in dense images. Since the centrality, dispersion, and asymmetry of the data are measured by the box plot, it is expected that the IQR varies in the SEM images. The evidence proved that the IQR of sparse images is more than dense images. In addition, the sparse VA-CNTs have a smoothness higher than the dense VA-CNTs. Intuitively, the

higher agglomeration in VA-CNTs images causes a higher PL amount. Besides, the greater uniformity and regularity of the nanoparticles decrease the PL amount. Thus, PL in sparse images is larger than in dense images. Furthermore, the sparse VA-CNTs have an E1 and E3 lower than the dense VA-CNTs. This situation occurs for Corr2 inversely.

Since it was necessary to set the two parameters of gamma and C in the SVM method, the best performances of gamma and C parameters were achieved by implementing ten times validation. Besides, several types of kernels of this method (i.e., linear, radial, and loop kernels) have been examined for the SVM model. Finally, the obtained accuracy of the variety of kernels was close to each other and did not differ significantly. Then, 80 images have been classified into two groups dense and sparse. Fig. 6 depicts the results obtained via training data from 0 to 40. As shown in Fig. 6, the best value for training data was 30 at a close accuracy of 98 percent. This accuracy demonstrated that VA-CNTs images could be separated.

The surface below the ROC curve is another criterion for assessing the proposed algorithm. This issue confirmed the accuracy of the classifier for the correct classification of up to 98%. In addition to the ROC curves, precision and accuracy indices were calculated. Table 6 gives the results of these indices and their corresponding components. All mentioned cases in Table 6 have been obtained from the confusion matrix. This issue shows the precision of the desired proposed algorithm. In Fig. 7, the ascending trend of the curve indicates that one can ensure the high performance of the diagnostic system with the test dataset and any other new dataset. According to the predictions, this method can assign each VA-CNTs image to its class with a 98% accuracy.

4 Conclusions

SVMs are recognized as a promising non-linear, non-parametric classification technique in machine learning. These methods can produce accurate and robust classification results even when the input data are non-monotone and non-linearly separable. Therefore, they can help conveniently evaluate more relevant information. In a set of training examples, each one is marked as belonging to one or the other of two categories. An SVM training algorithm builds a model that assigns new examples to a category or the other one. This situation makes it a non-probabilistic binary linear classifier. The present study proposed a new method to classify VA-CNTs SEM images. According to the time series and GLCM analysis, it was found that the specifications related to the dense VA-CNT images with standard deviations, Pearson law, skewness, correlation 2, and smoothness were low. But these images had high Energy 1, Energy 3, and IQR. Indeed, the standard deviations, Pearson law, skewness, correlation 2, smoothness, low Energy 1, Energy 3, and IQR are the specification attributes in bad images. The proposed algorithm has been tested on 80 VA-CNTs SEM images with identical sizes. The findings demonstrated a 98% precision, which proved the algorithm’s validity. The study contributions can be summarized as two parts: (I) developing a new method for extracting time series of VA-CNT images and (II) suggesting a new method for classifying VA-CNTs. These results demonstrated the high performance of the proposed algorithm to classify the mentioned images.

5 References

1. M. Endo, M. S. Strano, and P. M. Ajayan, "Potential applications of carbon nanotubes," in *Carbon nanotubes*: Springer, 2007, pp. 13-62.
2. Y. Yang, H. Zhang and Y. Yan, "Synthesis of CNTs on stainless steel microfibrous composite by CVD: Effect of synthesis condition on carbon nanotube growth and structure," *Composites Part B,* vol. 160, pp. 369-383, 2019.
3. M. S. Konsta-Gdoutos, Z. S. Metaxa, and S. P. Shah, "Highly dispersed carbon nanotube reinforced cement based materials," *Cement and Concrete Research,* vol. 40, no. 7, pp. 1052-1059, 2010.
4. P.-L. Chang, C.-C. Wu, and H.-J. Leu, "Using patent analyses to monitor the technological trends in an emerging field of technology: a case of carbon nanotube field emission display," *Scientometrics,* vol. 82, no. 1, pp. 5-19, 2010.

5. H. Cai, X. Cao, Y. Jiang, P. He, and Y. Fang, "Carbon nanotube-enhanced electrochemical DNA biosensor for DNA hybridization detection," *Analytical and bioanalytical chemistry,* vol. 375, no. 2, pp. 287-293, 2003.
6. Z. Liu, S. Tabakman, K. Welsher, and H. Dai, "Carbon nanotubes in biology and medicine: in vitro and in vivo detection, imaging and drug delivery," *Nano research,* vol. 2, no. 2, pp. 85-120, 2009.
7. P. J. F. Harris, *Carbon nanotube science: synthesis, properties and applications*. Cambridge university press, 2009.
8. Venkataraman, E. Victoria Amadi, Y. Chen and C. Papadopoulos, "Carbon Nanotube Assembly and Integration for Applications," *Nanoscale Research Letters,* vol. 14, no. 220, pp. 1-47, 2019.
9. N. Anzar, R. Hasan, M. Tyagi, N. Yadav and J. Narang, "Carbon nanotube - A review on Synthesis, Properties and plethora of applications in the field of biomedical science," *Sensors International,* vol. 1, no. 100003, pp. 1-10, 2020.
A. Jorio and R. Saito, "Raman spectroscopy for carbon nanotubeapplications," *Journal of Applied Physics,* vol. 129, no. 021102, pp. 1-27, 2021.
10. V. Schroeder, S. Savagatrup, M. He, S. Lin, and T. M. Swager, "Carbon Nanotube Chemical Sensors," *Chemical Reviews,* vol. 119, pp. 599-663, 2019.
11. P. Koirala, N. v. d. Werken, H. Lu, R. H. Baughman, R. Ovalle-Robles, M. Tehrani, " Using ultra-thin interlaminar carbon nanotube sheets to enhance the mechanical and electrical properties of carbon fiber reinforced polymer composites," *Composites Part B,* vol. 216, no. 108842, pp. 1-7, 2021.
12. K. R. Jinkins, S. M. Foradori, V. Saraswat, R. M. Jacobberger, J. H. Dwyer, P. Gopalan, A. Berson, M. S. Arnold, " Aligned 2D carbon nanotube liquid crystals for wafer-scale electronics," *science Advances,* vol. 7, pp. 1-11, 2021.
13. Y. Ahn, S. J. Kim, J. W. Jeong, S. Park, J. W. Kim, E. Go, J. W. Lee, J. T. Kang, K. N. Yun, S. Choi, S. Kim, J. H. Yeon, Y. H. Song, "Overall control of field emission from carbon nanotube paste-emitters through macro-geometries for high-performance electron source applications," *Carbon,* vol. 189, pp. 519-529, 2022.
14. F. M. Kochetkov, V. Neplokh, V. A. Mastalieva, S. Mukhangali, A. A. Vorob'ev, A. V. Uvarov, F. E. Komissarenko, D. M. Mitin, A. Kapoor, J. Eymery, N. Amador-Mendez, C. Durand, D. Krasnikov, A. G. Nasibulin, M. Tchernycheva and I. S. Mukhin, "Stretchable Transparent Light-Emitting Diodes Based on InGaN/GaN QuantumWell Microwires and Carbon Nanotube Films," *Nanomaterials,* vol. 11, no. 1503, pp. 1-10, 2021.
15. L. Xiang, Y. Hu, "Carbon Nanotube Dual-Material Gate Devices for Flexible Electronics," in *Nanoporous Carbons for Soft and Flexible Energy Devices,* Springer, 2022, pp. 23-41.
16. J. Han, J. Nam, S. Seo, A. Lee, C. Lee, S. Park, Y. Kang, H. Lee, D. Kim, Q. Zhang, H. Sung, E. I. Kauppinen, H. Jeong, J. Oh, S. Maruyama, I. D. Jung and I. Jeon, " Utilization of Multifunctional Environment-Friendly Organic Dopants Inspired from Nature for Carbon Nanotube-Based Planar Heterojunction Silicon Solar Cells," *Advanced Energy and Sustainability Research*, vol. 2100155, pp. 1-8, 2021.
17. S. K. Mishra, S. N. Tripathi, V. Choudhary, and B. D. Gupta, "Surface plasmon resonance-based fiber optic methane gas sensor utilizing graphene-carbon nanotubes-poly (methyl methacrylate) hybrid nanocomposite," *Plasmonics,* vol. 10, no. 5, pp. 1147-1157, 2015.
18. T. Hemraj-Benny *et al.*, "Synthesis and characterization of novel hybrids of tris [3-(trimethoxysilyl) propyl] isocyanurate (TTPI) capped palladium nanoparticles and single-walled carbon nanotubes," *Silicon,* vol. 3, no. 2, pp. 97-101, 2011.
19. S. Ahmad, "Aerosol CVD synthesis and applications of single-walled carbon nanotube thin films using spark-discharged produced catalyst," *Doctoral Dissertations*, Aalto University, School of Science, Department of Physics, NanoMaterials Group, 2020.
A. M. Mostafa, E. A. Mwafy and A. Toghan, "ZnO nanoparticles decorated carbon nanotubes via pulsed laser ablation method for degradation of methylene blue dyes," *Colloids and Surfaces A: Physicochemical and Engineering Aspects,* vol. 627, no. 127204, pp. 1-8, 2021.

20. S. Kang, H. Han, S. Mhin, H. R. Chae, W. R. Kim and K. M. Kim, "Ni-doped carbon nanotubes fabricated by pulsed laser ablation in liquid as efficient electrocatalysts for oxygen evolution reaction," *Applied Surface Science,* vol. 547, no. 149197, pp. 1-5, 2021.
A. A. Almarasy, T. Hayasaki, Y. Abiko, Y. Kawabata and S. Akasaka, A. Fujimori, "Comparison of characteristics of single-walled carbon nanotubes obtained by super-growth CVD and improved-arc discharge methods pertaining to interfacial film formation and nanohybridization with polymers," *Colloids and Surfaces A: Physicochemical and Engineering Aspects,* vol. 615, no. 126221, pp. 1-12, 2021.
21. L. M. Hoyos-Palacioa, D. P. C. Castrob, I. C. Ortiz-Trujillo, L. E. B. Palacioa, B. J. G. Upeguic, N. J. E. Morac and J. A. C. Corneliod, "Compounds of carbon nanotubes decorated with silver nanoparticles via in-situ by chemical vapor deposition (CVD)," *Journal of Materials Research and Technology,* vol. 8, no. 6, pp. 5893-5898, 2019.
22. M. Akter, E. Haque, M. Parvez and A. Matin, " Synthesis of Carbon Nanotube by Chemical Vapor Deposition (CVD) Method," *Scientific Research Journal,* vol. VIII, no. VI, pp. 30-33, 2020.
23. B. Mahdavipour and A. S. Elahi, "Growth and Characterization of Boron-Carbon Structures with the Hot Filament Chemical Vapor Deposition Technique," *Silicon,* pp. 1-6, 2018.
24. S. Izadyar, M. R. Hantehzadeh, M. Ghoranneviss, S. M. Elahi, and A. Boochani, "Prevailing Cu-C Nanocomposite over Cu NPs for CNTs Growth: A Catalyst Study on Silicon Substrate," *Silicon,* pp. 1-6, 2017.
25. M. Kumar and Y. Ando, "Chemical vapor deposition of carbon nanotubes: a review on growth mechanism and mass production," *Journal of nanoscience and nanotechnology,* vol. 10, no. 6, pp. 3739-3758, 2010.
26. C. Lu, F. Shi, J. Jin and X. Peng, "Study on the Properties of Vertical Carbon Nanotube Films Grown on Stainless Steel Bipolar Plates," *Materials,* vol. 12, no. 899, pp. 1-15, 2019.
27. E. L. M. Pereira, A. S. M. Batista, F. A. S. Ribeiro, A. P. Soares, A. H. Oliveira, H. Arno and L. O. Faria, "Scanning Electron Microscope Evaluation of the Poly (vinylidene fluoride)/Multiple-Walled Carbon Nanotubes-Metal Oxides Nanocomposites," *Materials Focus,* vol. 7, no. 3, pp. 333-337, 2018.
28. N. Liu, X. Chen, J. Zhang, and J. W. Schwank, "A review on TiO2-based nanotubes synthesized via hydrothermal method: Formation mechanism, structure modification, and photocatalytic applications," *Catalysis Today,* vol. 225, pp. 34-51, 2014.
29. J. Prasek *et al.*, "Methods for carbon nanotubes synthesis," *Journal of Materials Chemistry,* vol. 21, no. 40, pp. 15872-15884, 2011.
30. S. Kalaiselvan, K. Balachandran, S. Karthikeyan, and R. Venckatesh, "Botanical Hydrocarbon Sources based MWCNTs Synthesized by Spray Pyrolysis Method for DSSC Applications," *Silicon,* vol. 10, no. 2, pp. 211-217, 2018.
31. K. Hata, D. N. Futaba, K. Mizuno, T. Namai, M. Yumura, and S. Iijima, "Water-assisted highly efficient synthesis of impurity-free single-walled carbon nanotubes," *Science,* vol. 306, no. 5700, pp. 1362-1364, 2004.
32. Z. Ghorannevis, E. Akbarnejad, B. Aghazadeh, and M. Ghoranneviss, "Decoration of MWCNTs by CdS Nanoparticles Using Magnetron Sputtering Method," *Silicon,* pp. 1-6, 2017.
33. R. Kumar, A. V. Alaferdov, R. K. Singh, A. K. Singh, J. Shah, R. K. Kotnala, K. Singh, Y. Suda and S. A. Moshkalev, "Self-assembled nanostructures of 3D hierarchical faceted-iron oxide containing vertical carbon nanotubes on reduced graphene oxide hybrids for enhanced electromagnetic interface shielding," *Composites Part B,* vol. 168, pp. 66-76, 2019.
34. H. Rennhofer and B. Zanghellini, "Dispersion State and Damage of Carbon Nanotubes and Carbon Nanofibers by Ultrasonic Dispersion: A Review," *nanomaterials,* vol. 11, no. 1469, pp. 1-27, 2021.
35. V. Trovato, E. Teblum, Y. Kostikov, A. Pedrana, V. Re, G. D. Nessim and G. Rosace, "Electrically conductive cotton fabric coatings developed by silica sol-gel precursors doped with surfactant-aided dispersion of vertically aligned carbon nanotubes fillers in organic solvent-free aqueous solution," *Journal of Colloid and Interface Science,* vol. 586, pp. 120-134, 2021.

36. H. Zhang, B. Wang and B. Brown, "Atomic layer deposition of titanium oxide and nitride on vertically aligned carbon nanotubes for energy dense 3D microsupercapacit," *Applied Surface Science,* vol. 521, no. 146349, pp. 1-8, 2020.
37. K. Tanaka, "Classification of Carbon," in *Carbon Nanotubes and Graphene (Second Edition)*: Elsevier, 2014, pp. 1-5.
38. W.C. Su and Y. S. Cheng, "Carbon nanotubes size classification, characterization and nasal airway deposition," *Inhalation toxicology,* vol. 26, no. 14, pp. 843-852, 2014.
39. H.-J. Bunge, *Texture analysis in materials science: mathematical methods*. Elsevier, 2013.
40. M. H. Bharati, J. J. Liu, and J. F. MacGregor, "Image texture analysis: methods and comparisons," *Chemometrics and intelligent laboratory systems,* vol. 72, no. 1, pp. 57-71, 2004.
41. W. W. Wei, "Time series analysis," in *The Oxford Handbook of Quantitative Methods in Psychology: Vol. 2*, 2006.
42. E. Gadelmawla, "A vision system for surface roughness characterization using the gray level co-occurrence matrix," *NDT & e International,* vol. 37, no. 7, pp. 577-588, 2004.
43. D. Freitag, "Machine learning for information extraction in informal domains," *Machine learning,* vol. 39, no. 2-3, pp. 169-202, 2000.
44. Y. Li, C. Guan, H. Li, and Z. Chin, "A self-training semi-supervised SVM algorithm and its application in an EEG-based brain computer interface speller system," *Pattern Recognition Letters,* vol. 29, no. 9, pp. 1285-1294, 2008.
45. X. Wu *et al.*, "Top 10 algorithms in data mining," *Knowledge and information systems,* vol. 14, no. 1, pp. 1-37, 2008.
46. K. M. Ting, "Confusion matrix," in *Encyclopedia of Machine Learning and Data Mining*: Springer, 2017, pp. 260-260.
47. D. K. McClish, "Analyzing a portion of the ROC curve," *Medical Decision Making,* vol. 9, no. 3, pp. 190-195, 1989.

Table 1 Textural features used in paper

Histogram Intensity		**GLCM [36]**
Mean	**Pearson Law**	**Energy**
$M = \sum_{i=0}^{L-1} z_i p(z_i)$	$PL = \lvert 3(M - Median)(p(z_i)) - (M - \mathrm{mod})(p(z_i)) \rvert$	$E = \sum_{i=0}^{N-1}\sum_{j=0}^{N-1} pix(i,j)^2$
Variance	**Kurtosis**	
$v = \sum_i \sum_j (i-\mu)^2 pix(i,j)$	$Ku = \sum_{i=0}^{L-1} (z_i - m)^4 p(z_i)$	**Homogeneity**
Moment	**Mode**	$Homo = \sum_{i=0}^{N-1}\sum_{j=0}^{N-1} \frac{pix(i,j)}{1+\lvert i-j \rvert}$
$Moment = \sum_{i=0}^{L-1} (z_i - m)^4 p(z_i)$	$Mod = \underset{z_i}{\mathrm{mod}}\{p(z_i)\}$	
Standard Deviation	**Median**	**Correlation**
$STD = \sqrt{\mu_2}$	$Median = \underset{z_i}{median}\{p(z_i)\}$	$Corr = \sum_{i=0}^{N-1}\sum_{j=0}^{N-1} \frac{(i-\mu_x)(j-\mu_y)pix(i,j)}{\sigma_x \sigma_y}$
Smoothness	**IQR**	**Contrast**
$Sm = 1 - \frac{1}{1+\mu_2}$	$IQR = \underset{z_i}{quar3}\{p(z_i)\} - \underset{z_i}{quar1}\{p(z_i)\}$	

Skewness

$$Sk = \sum_{i=0}^{L-1}(z_i - m)^3 p(z_i)$$

Entropy

$$Ent = -\sum_{i=0}^{N-1}\sum_{j=0}^{N-1} pix(i,j)\log(pix(i,j))$$

$$Cont = \sum_{i=0}^{N-1}\sum_{j=0}^{N-1}|i-j|^2 pix(i,j)$$

Max

Inertia

$$In = \sum_{i=0}^{N-1}\sum_{j=0}^{N-1}(i-j)^2 pix(i,j)$$

Table 2 Confusion Matrix

	Predicted Positive	Predicted Negative
True Negative	FP	TN
True Positive	TP	FN

Table 3 Dispersion of different features for the SEM images of CNTs

	Features	**Dense**	**Sparse**
		Mean ± STD	**Mean ± STD**
1	Mean	114.86 ± 20.29	100.57 ± 23.19
2	Mode	103.72 ± 28.29	69.38 ± 27.95
3	Median	113.79 ± 20.54	94.19 ± 23.92
4	Moment	0.25 ± 0.03	0.20 ± 0.05
5	**Standard Deviation (*STD*)**	**20.93 ± 7.58**	**38.12 ± 7.74**
6	Covariance	19.05 ± 7.65	32.07 ± 13.48
7	**Pearson Law (*PL*)**	**9.95 ± 6.82**	**27.41 ± 8.09**
8	**Skewness (*Sk*)**	**0.30 ± 0.16**	**1.03 ± 0.39**
9	Kurtosis	2.96 ± 0.50	2.87 ± 0.84
10	Contrast1	0.21 ± 0.13	0.26 ± 0.17
11	Correlation1	0.26 ± 0.12	0.31 ± 0.13
12	**Energy1 (*E*1)**	**0.27 ± 0.05**	**0.19 ± 0.03**
13	Homogeneiy1	0.90 ± 0.05	0.90 ± 0.04
14	Inertia1	0.46 ± 0.17	0.41 ± 0.13
15	Contrast2	0.24 ± 0.14	0.31 ± 0.22
16	**Correlation2 (*Corr*2)**	**0.78 ± 0.06**	**0.86 ± 0.03**
17	Energy2	0.29 ± 0.13	0.25 ± 0.12
18	Homogeneiy2	0.89 ± 0.05	0.87 ± 0.06
19	Inertia2	0.45 ± 0.17	0.40 ± 0.13

20	Contrast3	0.11 ± 0.05	0.14 ± 0.08
21	Correlation3	0.87 ± 0.05	0.91 ± 0.06
22	**Energy3 (*E*3)**	**0.29 ± 0.05**	**0.19 ± 0.06**
23	Homogeneiy3	0.95 ± 0.02	0.94 ± 0.03
24	Inertia3	0.49 ± 0.16	0.43 ± 0.13
25	Contrast4	0.24 ± 0.13	0.29 ± 0.18
26	Correlation4	0.78 ± 0.10	0.84 ± 0.08
27	Energy4	0.30 ± 0.15	0.24 ± 0.12
28	Homogeneiy4	0.89 ± 0.06	0.87 ± 0.06
29	Inertia4	0.40 ± 0.13	0.40 ± 0.13
30	**Smoothness (*Sm*)**	**0.009 ± 0.008**	**0.04 ± 0.01**
31	**Inter Quartile Range (*IQR*)**	**65.32 ± 14.31**	**41.04 ± 10.28**
32	Entropy	6.26 ± 0.51	6.36 ± 0.60

Table 4 The values of features for images of Fig. 4

	Features							
image	**STD**	**PL**	**Sk**	**IQR**	**Sm**	**E1**	**Corr2**	**E3**
a	40.90	19.38	1.05	40.09	0.03	0.24	0.91	0.21
b	46.53	24.76	0.69	52.36	0.03	0.17	0.93	0.19
c	47.03	21.12	0.70	38.91	0.03	0.19	0.90	0.21
d	40.67	19.72	0.59	30.85	0.02	0.19	0.92	0.18
e	44.23	14.86	1.08	54.47	0.03	0.11	0.87	0.15
f	46.22	29.47	0.70	41.26	0.03	0.15	0.92	0.18
g	47.27	44.66	0.56	31.74	0.03	0.16	0.91	0.21
h	51.51	28.38	0.70	46.50	0.04	0.16	0.95	0.19
i	28.39	33.34	1.11	42.83	0.01	0.20	0.91	0.31

Table 5 The values of features for images of Fig. 5

	Features							
image	**STD**	**PL**	**Sk**	**IQR**	**Sm**	**E1**	**Corr2**	**E3**
a	30.70	19.48	0.29	71.52	0.010	0.19	0.76	0.24
b	33.52	5.70	0.33	62.84	0.021	0.22	0.83	0.20
c	24.58	6.03	0.39	47.90	0.008	0.21	0.62	0.27
d	27.54	8.64	0.28	54.33	0.009	0.19	0.80	0.25
e	30.70	19.48	0.49	56.45	0.009	0.26	0.76	0.24

f	19.68	4.19	0.48	63.15	0.012	0.30	0.80	0.34
g	24.83	14.89	0.36	69.76	0.015	0.34	0.65	0.27
h	17.96	14.47	0.24	72.20	0.019	0.30	0.78	0.35
i	22.05	8.02	0.13	59.96	0.009	0.26	0.80	0.28

Table 6 The summary results of the index ROC curve, accuracy and kappa coefficient in SVM

Index	Value
Sensitivity	1
Specificity	0.96
Pos Pred Value	1
Neg Pred Value	0.96
Accuracy	0.98
Kappa	0.90
AUC	0.97

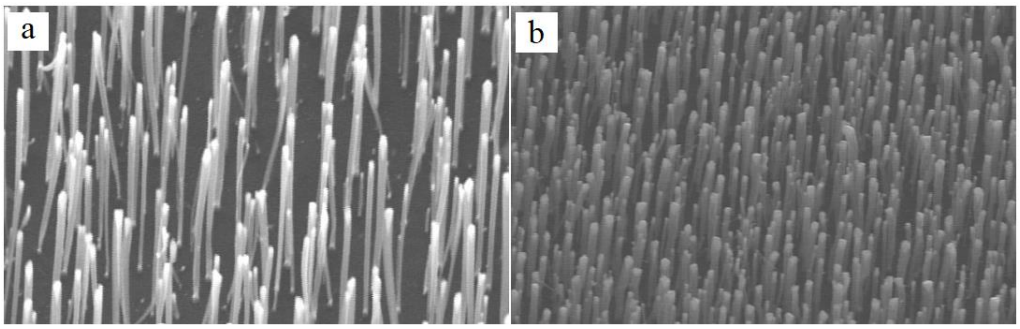

Fig. 1 The SEM images of CNTs. (a) Sparse image, (b) Dense image

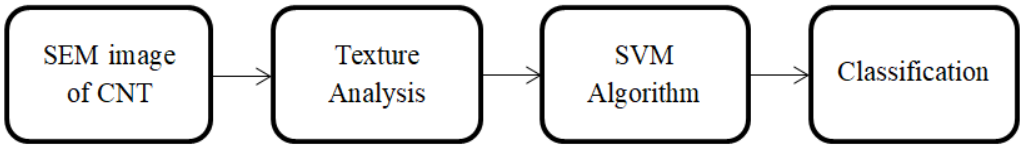

Fig. 2 The block diagram for classification of CNT images

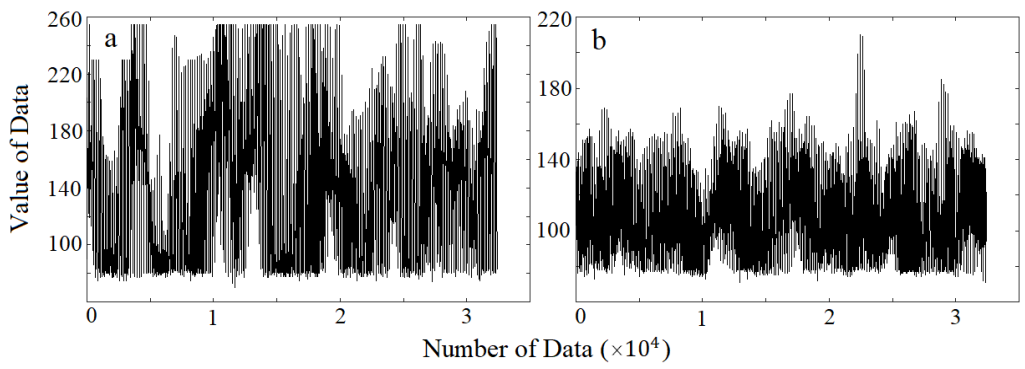

Fig. 3 The time series of SEM image of CNTs in Fig. 1
(a) The time series of Fig. 1(a), (b) The time series of Fig. 1(b)

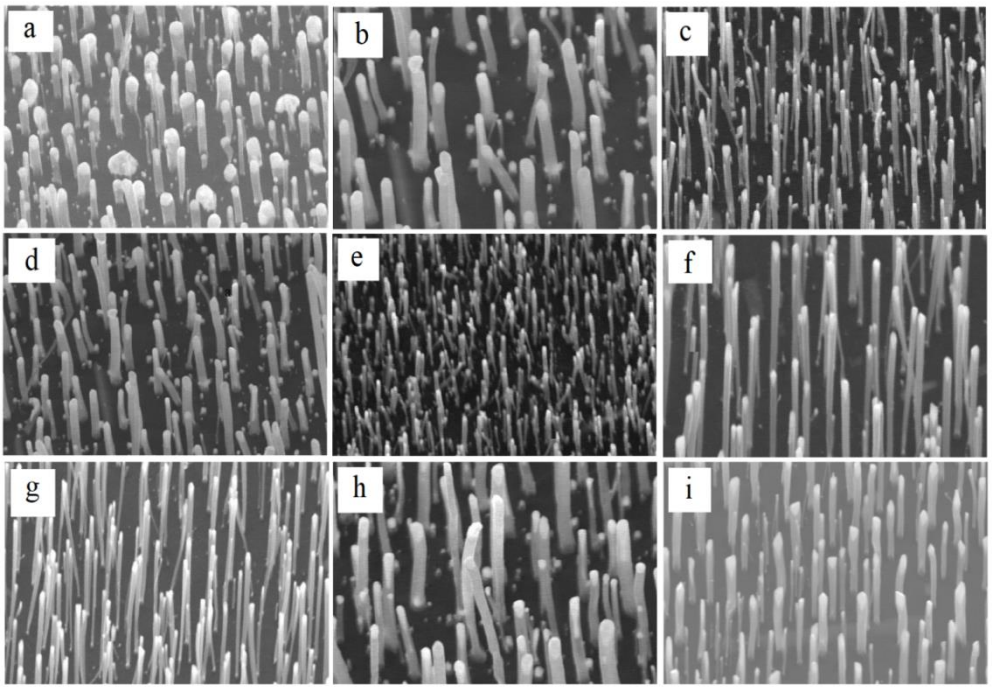

Fig.4 The examples of sparse SEM images of CNTs

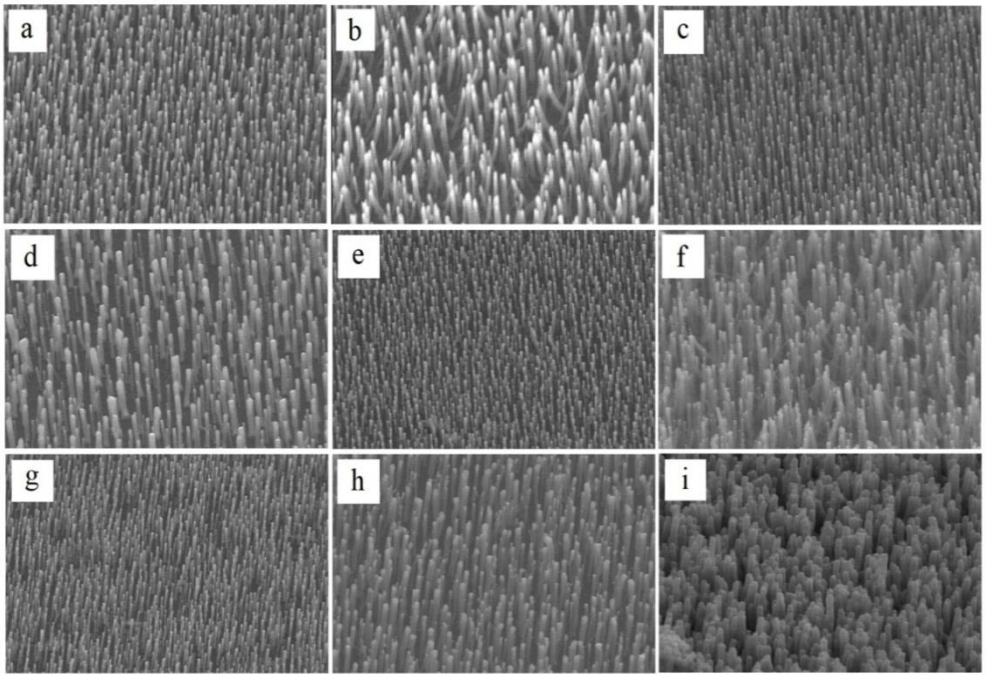

Fig.5 The examples of dense SEM images of CNTs

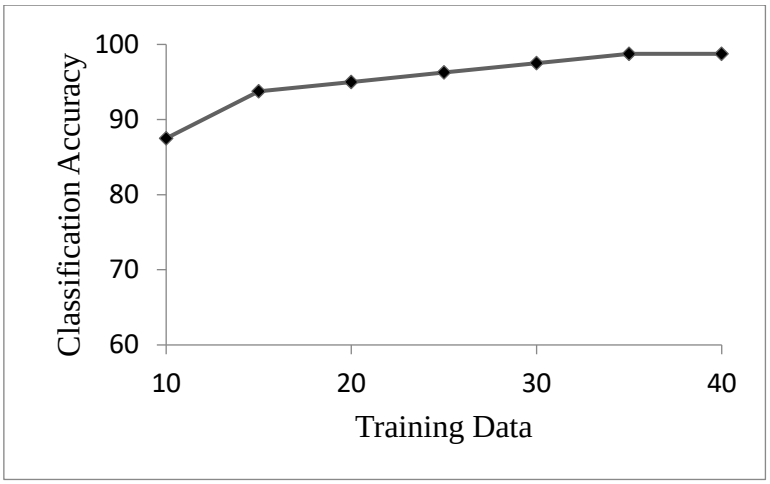

Fig. 6 The results of classification accuracy for different ratios of training and test data

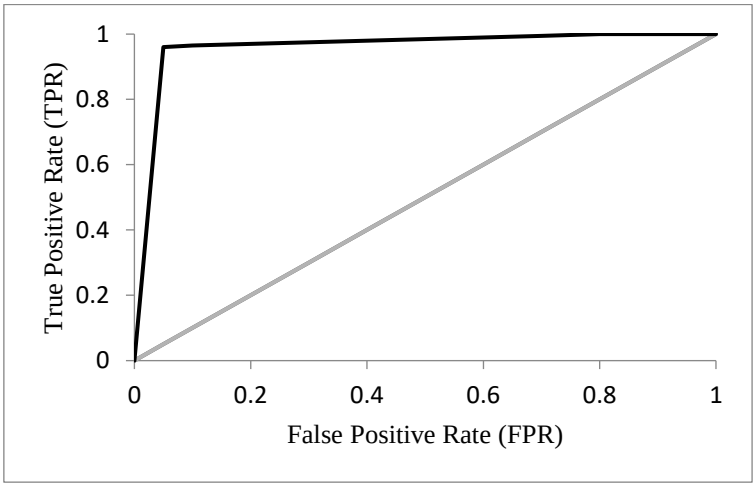

Fig. 7 The ROC curve of SVM classifier